Relative CO_2/NH_3 selectivities of AQP1, AQP4, AQP5, AmtB, and RhAG

Raif Musa-Aziz[a,b,1,2], Li-Ming Chen[a,b,2], Marc F. Pelletier[a,c], and Walter F. Boron[a,b,1]

[a]Department of Cellular and Molecular Physiology, Yale University School of Medicine, New Haven, CT 06520; [c]Aeromics, LLC, Cleveland, OH 44106; and [b]Department of Physiology and Biophysics, Case Western Reserve University, Cleveland, OH 44106

Communicated by Gerhard Giebisch, Yale University School of Medicine, New Haven, CT, December 30, 2008 (received for review November 18, 2008)

The water channel aquaporin 1 (AQP1) and certain Rh-family members are permeable to CO_2 and NH_3. Here, we use changes in surface pH (pH_S) to assess relative CO_2 vs. NH_3 permeability of *Xenopus* oocytes expressing members of the AQP or Rh family. Exposed to CO_2 or NH_3, AQP1 oocytes exhibit a greater maximal magnitude of pH_S change (ΔpH_S) compared with day-matched controls injected with H_2O or with RNA encoding SGLT1, NKCC2, or PepT1. With CO_2, AQP1 oocytes also have faster time constants for pH_S relaxation (τ_{pHs}). Thus, AQP1, but not the other proteins, conduct CO_2 and NH_3. Oocytes expressing rat AQP4, rat AQP5, human RhAG, or the bacterial Rh homolog AmtB also exhibit greater $\Delta pH_S(CO_2)$ and faster τ_{pHs} compared with controls. Oocytes expressing AmtB and RhAG, but not AQP4 or AQP5, exhibit greater $\Delta pH_S(NH_3)$ values. Only AQPs exhibited significant osmotic water permeability (P_f). We computed channel-dependent (*) ΔpH_S or P_f by subtracting values for H_2O oocytes from those of channel-expressing oocytes. For the ratio $\Delta pH_S(CO_2)^*/P_f^*$, the sequence was AQP5 > AQP1 ≅ AQP4. For $\Delta pH_S(CO_2)^*/\Delta pH_S(NH_3)^*$, the sequence was AQP4 ≅ AQP5 > AQP1 > AmtB > RhAG. Thus, each channel exhibits a characteristic ratio for indices of CO_2 vs. NH_3 permeability, demonstrating that, like ion channels, gas channels can exhibit selectivity.

gas channel | oocyte | permeability | signal peptide | surface pH measurement

Gas transport through membranes is of fundamental importance for nutritive transport, photosynthesis, oxidative metabolism, and signaling. For most of the past century, we assumed that gas molecules cross biological membranes merely by diffusing through the lipid phase. This dogma was challenged by 2 observations: (*i*) Apical membranes of gastric-gland cells have no demonstrable permeability to CO_2 or NH_3 (1). (*ii*) Heterologous expression of the water channel aquaporin 1 (AQP1) increases the CO_2 permeability of *Xenopus* oocytes (2). Cooper and Boron (3) and Prasad *et al.* (4) confirmed and extended this observation. Uehlein (5) showed that an AQP plays a physiological role by enhancing CO_2 uptake by plants. Endeward *et al.* (6) demonstrated that AQP1 accounts for ≈60% of the CO_2 permeability of human red blood cells (RBCs). Molecular dynamics simulations suggest that CO_2 can pass through the 4 aquapores of an AQP1 tetramer (7) and especially through the central pore between the 4 monomers (7). Additional data indicate that AQP1 is permeable to nitric oxide (8), and that—when expressed in *Xenopus* oocytes (9, 10) or when reconstituted into planar lipid bilayers (11)—AQP1, AQP3, AQP8, AQP9, and the plant aquaporin TIP2;1 are all permeable to NH_3.

The AmtB/MEP/Rh proteins represent a second family of gas channels (12–15). Early work showed that AmtB and MEP transport NH_3 or NH_4^+, thereby playing a nutritive role in archaea, bacteria, and fungi (16, 17). The crystal structures of the bacterial AmtB (18–20) and Rh50 (21) and the fungal Amt-1 (22) are consistent with the idea that NH_3 passes through a pore in each monomer of the homotrimer. Indeed, reconstituted AmtB conducts NH_3 (14), and RhAG is necessary for NH_3 transport in mammalian RBCs (23). Soupene *et al.* found that Rh1 deficiency impairs the growth of the green alga *C. reinhardtii* (24) and suggested that Rh1 plays a role in CO_2 transport. In RBCs, RhAG accounts for ≈50% of CO_2 transport (25).

In 2006, we introduced an approach (6) to assess CO_2 transport by pushing a blunt microelectrode against the surface of an oocyte, while monitoring surface pH (pH_S). Introducing extracellular CO_2 causes a transient pH_S increase, the maximum magnitude of which (ΔpH_S) is an index of maximal CO_2 influx. Earlier, De Hemptinne and Huguenin (26) had observed such a CO_2-induced transient while monitoring extracellular pH (pH_o) of rat soleus muscle. Moreover, Chesler (27) had found that exposing lamprey neurons to NH_3 causes a transient decreases in pH_o. Here, we exploit CO_2- and NH_3-induced pH_S transients to study the CO_2 vs. NH_3 permeability of 4 channels abundantly expressed in cells that mediate high rates of gas transport: human AQP1 (RBCs; ref. 28), the M23 variant of rat AQP4 (astrocytic endfeet at the blood–brain barrier, ref. 29), rat AQP5 (alveolar type I pneumocytes; ref. 30), and human RhAG (RBCs, ref. 31). We also studied bacterial AmtB. Our results show that all 5 channels are permeable to CO_2, and all but AQP4 and AQP5 are permeable to NH_3. A relative index of CO_2/NH_3 permeability varied widely: AQP4 ≅ AQP5 > > AQP1 > AmtB > RhAG. Thus, as is true for ion channels, gas channels exhibit substantial solute selectivity, which could play an important physiological role in controlling gas fluxes.

Results

pH_S Transients Caused by Applying CO_2 vs. NH_3. Fig. 1*A* illustrates schematically how the influx of CO_2 leads to a fall in $[CO_2]$ near the extracellular surface of the membrane ($[CO_2]_S$), which in turn leads to a rise in pH_S. Fig. 1*B* shows how the influx of NH_3 leads to a fall in pH_S. As described in ref. 6, exposing an AQP1-expressing oocyte to a solution containing 5% CO_2/33 mM HCO_3^- at a constant pH of 7.50 causes a transient rise in pH_S, followed by an exponential decay (Fig. 1*C Left*, green record). After the washout of CO_2 (see *SI Text* and Fig. S3), exposing the same oocyte to 0.5 mM NH_3/NH_4^+ causes a transient fall in pH_S (Fig. 1*C Right*, green record), as noted elsewhere (32). Additional data are consistent with the hypothesis that *Xenopus* oocytes handle NH_3 in an unusual way, sequestering most incoming NH_3 in an intracellular compartment as NH_4^+ (32).

The maximal pH_S transients are much smaller in day-matched oocytes injected with H_2O (orange) or cRNA encoding the Na/glucose cotransporter SGLT1 (black), and are totally lacking

Author contributions: R.M.-A., L.-M.C., M.F.P., and W.F.B. designed research; R.M.-A., L.-M.C., and M.F.P. performed research; R.M.-A. analyzed data; and R.M.-A., L.-M.C., and W.F.B. wrote the paper.

The authors declare no conflict of interest.

[1]To whom correspondence may be addressed. E-mail: raif.aziz@case.edu or walter.boron@case.edu.

[2]R.M.-A. and L.-M.C. contributed equally to this work.

This article contains supporting information online at www.pnas.org/cgi/content/full/0813231106/DCSupplemental.

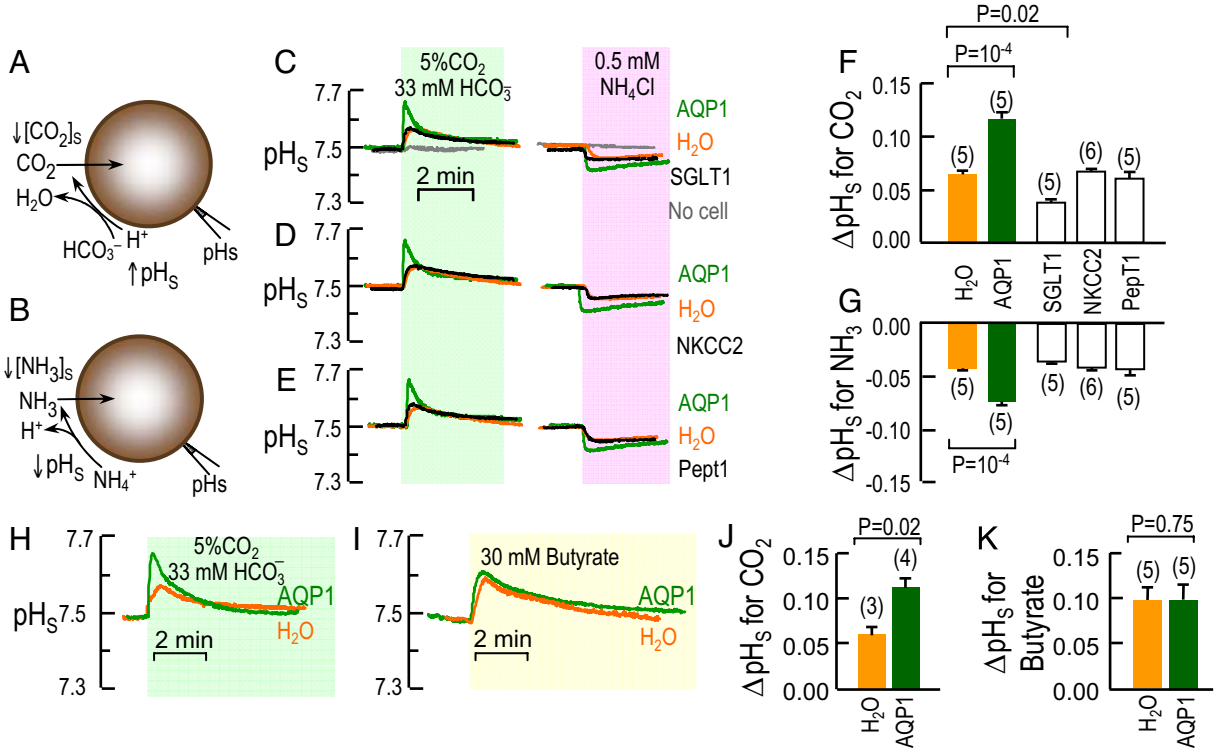

Fig. 1. Basis of surface pH changes. (*A*) CO_2 influx. At the outer surface of the membrane, the CO_2 influx creates a CO_2 deficit. The reaction $HCO_3^- + H^+ \rightarrow CO_2 + H_2O$, in part, replenishes the CO_2, raising pH_S. (*B*) NH_3 influx. The reaction $NH_4^+ \rightarrow NH_3 + H^+$, in part, replenishes NH_3, lowering pH_S. (*C–E*) Representative pH_S transients from oocytes injected with H_2O or expressing AQP1 (record repeated in the 3 images), SGLT1, NKCC2, or PepT1. All data in *C–E* were obtained on the same day, from the same batch of oocytes, exposed first to CO_2/HCO_3^- and then (after CO_2 removal) to NH_3/NH_4^+. Also shown in *C* are records with no oocyte present. Before and after solution changes, we retracted the pH electrode to the bulk extracellular solution (pH 7.50) for calibration. (*F* and *G*) Summary of extreme excursions of pH_S (ΔpH_S) for CO_2 and NH_3 data. (*H* and *I*) Representative pH_S transients from day-matched H_2O or AQP1 oocytes exposed to CO_2/HCO_3^- or 30 mM butyrate. (*J* and *K*) Summary of ΔpH_S for experiments like those in *H* or *I*. Values are means ± SE, with numbers of oocytes in parentheses. For *F* and *G*, statistical comparison between H_2O-injected controls and other oocytes (separately for CO_2 and NH_3 data) were made using a 1-way ANOVA for 5 groups, followed by Dunnett's multiple comparison. ΔpH_S values for H_2O, NKCC2, and PepT1 do not differ from one other. For *J* and *K*, statistical comparisons were made using unpaired 2-tailed *t* tests.

in the absence of an oocyte (gray). Moreover, oocytes expressing the Na/K/Cl cotransporter NKCC2 or the H/oligopeptide cotransporter PepT1 have ΔpH_S values similar to those of H_2O-injected oocytes (Fig. 1 *D* and *E*).

Fig. 1 *F* and *G* summarize ΔpH_S data for a larger number of experiments like those in Fig. 1 *C–E* and show that ΔpH_S for AQP1 is significantly greater than for all other oocyte groups. As expected, the time constant (τ_{pHs}) for the decay of pH_S from its peak, an index of the time required for CO_2 to equilibrate across the membrane, has a pattern that is the inverse of that for ΔpH_S (Fig. S1 *A* and *B*). Because of the oocyte's unusual NH_3 handling, the pH_S relaxation during NH_3 exposures is prolonged, precluding the calculation of a τ_{pHs} for NH_3. In the CO_2 protocol, the smaller ΔpH_S for SGLT1 vs. H_2O oocytes could reflect a decrease in the expression of other proteins or an increase in membrane–protein/lipid ratio.

Given our observations with CO_2, one might ask whether AQP1 also would enhance the flux of a permeant weak acid like butyric acid (33). While confirming that AQP1 increases the ΔpH_S in oocytes exposed to CO_2 (Fig. 1 *H* and *J*), we found that the channel has no effect either on ΔpH_S (Fig. 1 *I* and *K*) or τ_{pHs} (Fig. S1 *C* and *D*) in oocytes exposed to butyric acid.

In principle, AQP1 could enhance the CO_2-induced pH_S spike in Fig. 1 *C* or *H*, not because AQP1 is a CO_2 channel, but because it has unanticipated carbonic anhydrase (CA) activity and thus catalyzes the extracellular reaction $HCO_3^- + H^+ \rightarrow CO_2 + H_2O$ (see Fig. 1*A*). To test the CA hypothesis, we injected oocytes with cRNA encoding CA IV, coupled via a GPI linkage to the outer surface of the membrane. Increased CA-IV expression causes a graded increase in ΔpH_S (Fig. S2), and we determined the dose of CA-IV cRNA that produces the same ΔpH_S as a typical AQP1 oocyte. Fig. 2 shows that membrane preparations of oocytes injected with this dose of CA-IV cRNA, compared with those from H_2O oocytes, require a much shorter time to achieve a pH endpoint in a CA assay. However, membrane preparations of AQP1 oocytes are indistinguishable from those

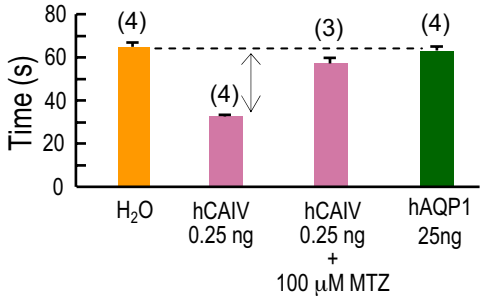

Fig. 2. Carbonic anhydrase activities of *Xenopus* oocytes. CA activity was determined from membrane preparations of 100 oocytes injected with H_2O, 0.25 ng of cRNA encoding hCA IV, or 25 ng of cRNA encoding hAQP1. We divided each membrane preparation into aliquots containing 20 μg of total protein and performed a colorimetric CA assay on each aliquot (see *SI Text*). The sample mixtures containing CA-IV were run ± 100 μM methazolamide (MTZ), a CA inhibitor. Each N refers to a CA assay on 1 aliquot.

PHYSIOLOGY

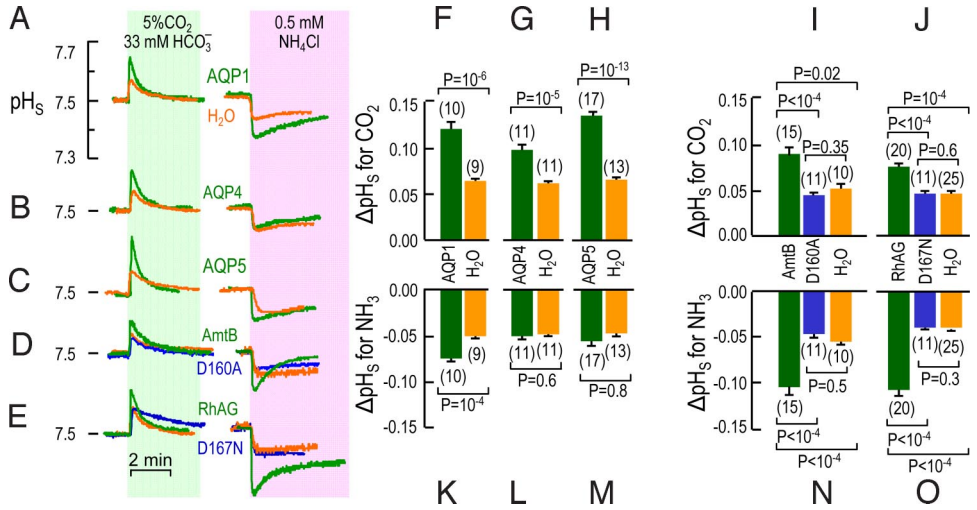

Fig. 3. Surface pH changes caused by CO_2 and NH_3 influx in oocytes expressing gas-channel proteins. (*A–E*) Typical pH_S transients from oocytes injected with H_2O or expressing AQP1, AQP4, AQP5, WT AmtB or its inactive D160A mutant, or WT RhAG or its inactive D167A mutant. The protocol was the same as in Fig. 1. (*F–J*) Summary of extreme excursions of pH_S (ΔpH_S) caused by CO_2 influx. Each image represents mean values for day-matched oocytes. (*K–O*) Summary of ΔpH_S caused by NH_3 influx. Each image (*F–O*) represents mean values for day-matched oocytes. Some H_2O oocytes served as controls in more than 1 panel (total number of H_2O oocytes: 54 for CO_2, 61 for NH_3). Values are means ± SE, with numbers of oocytes in parentheses. For *F–H* and *K–M*, statistical comparisons were made using unpaired 2-tailed *t* tests. For *I* and *J* and *N* and *O*, statistical comparisons were made using 1-way ANOVAs for 3 groups, followed by Student–Newman–Keuls analyses.

of H_2O, allowing us to rule out the CA hypothesis. Thus, on the basis of ΔpH_S and τ_{pHs} measurements, AQP1, but not SGLT1, NKCC1, and PepT1, acts as a channel for CO_2 and NH_3.

Comparison of AQPs with AmtB and RhAG. Using the same protocol shown in Fig. 1 *C–E*, we systematically examined the effects of sequential exposures to CO_2/HCO_3^- and then NH_3/NH_4^+ on oocytes expressing AQP1, AQP4, AQP5, AmtB, or RhAG. Fig. 3*A* shows again that CO_2 and NH_3 elicit larger pH_S spikes in AQP1 (green) than in day-matched H_2O (orange) oocytes. Both AQP4 (Fig. 3*B*) and AQP5 (Fig. 3*C*) enhance the pH_S spike with CO_2 but not with NH_3. Both AmtB (Fig. 3*D*) and RhAG (Fig. 3*E*) enhance the pH_S spike with CO_2 but are especially effective with NH_3. Asp^{160} is vital for AmtB activity (19, 34), and the homologous Asp^{167} is required by RhAG (35). We found that the inactive D160A mutant of AmtB (34, 36) and the inactive D167N mutant of RhAG (35) are inactive as either CO_2 or NH_3 channels, presumably because the mutations cause major structural changes (35). Figs. S3 and S4 *A* and *D* show full-length experiments similar to those in Fig. 3 *A–E*.

In the above experiments, all AmtB and RhAG constructs were C-terminally tagged with EGFP (enhanced GFP), and fluorescence measurements confirmed trafficking to near the oocyte surface. The tagged and untagged constructs yielded identical results in pH_S assays (Fig. S4).

Fig. 3 *F–J* are analogous to Fig. 1*F*, except that in Fig. 3 *F–J*, we pair each oocyte expressing a WT or mutant channel with its day-matched H_2O-injected control. Each WT protein yields a ΔpH_S that is significantly greater than the H_2O control or (as applicable) the mutant protein. Moreover, the ΔpH_S values of the mutants are not different from the corresponding H_2O oocytes. Fig. 3 *K–O* is a summary of the NH_3 data. The results are comparable to the CO_2 data, except that the magnitudes of ΔpH_S for AQP4 and AQP5 in the NH_3 protocol are not different from those of their corresponding H_2O-injected controls. Fig. S5 shows that the relationship for the τ_{pHs} values is the inverse of that for the ΔpH_S values in Fig. 3. Thus, each of the proteins, AQP1, AQP4, AQP5, AmtB, and RhAG, is permeable to CO_2. Moreover, AQP1, AmtB, and RhAG, but not AQP4 or AQP5, are permeable to NH_3.

Cleavage of AmtB Signal Peptide by Oocytes. Our AmtB cDNA encodes a signal peptide that *Escherichia coli* naturally cleaves (37), so that the new N terminus is extracellular. The A22K point mutation in AmtB prevents the cleavage in *E. coli*, although the mutant AmtB still forms trimers and is active (37). To verify that *Xenopus* oocytes also cleave the signal peptide, we added a C-terminal His tag to WT AmtB, A22K-AmtB, and an AmtB variant with the signal peptide truncated. Fig. 4 shows Western blots of plasma-membrane preparations from oocytes expressing the 3 constructs. The molecular mass of the major band of WT AmtB is appropriately less than that of A22K-AmtB, but the same as truncated AmtB. Thus, oocytes do indeed cleave the signal peptide of WT AmtB. Densitometry indicates that >90% of the AmtB in oocytes is appropriately cleaved. Additional data reveal that AmtB-His is active as both a CO_2 and an NH_3 channel.

P_f in Oocytes Expressing Different Channels. So that we could relate our CO_2 and NH_3 data to the wealth of information on the osmotic water permeability (P_f) of AQP-expressing oocytes, we determined P_f for each AQP oocyte and its day-matched control from the dataset in Fig. 3. As summarized by the 3 pairs of bars on the left side of Fig. 5, the mean P_f value for each AQP was significantly and substantially greater than the matched controls. We separately assessed P_f for matched oocytes expressing AQP1,

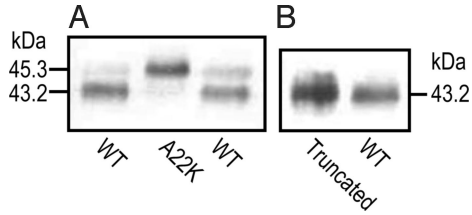

Fig. 4. Western blots testing cleavage of the AmtB signal peptide in *Xenopus* oocytes. (*A*) Wild-type AmtB vs. uncleavable A22K mutant. (*B*) Wild-type AmtB vs. AmtB with truncated signal peptide. Data are representative of 4 similar experiments. All constructs were His tagged at the C terminus and detected with an anti-His antibody.

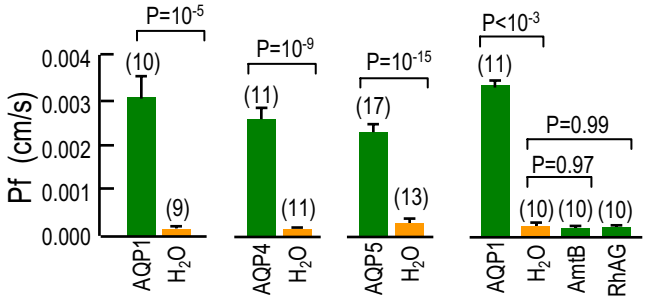

Fig. 5. Osmotic water permeabilities of *Xenopus* oocytes. P_f (cm/s) of oocytes injected with H_2O or cRNA encoding AQP1, AQP4, AQP5, AmtB, or RhAG. Values are means ± SE, with numbers of oocytes in parentheses. Statistical comparison between H_2O vs. AQP oocytes were made using unpaired 2-tailed *t* tests. Statistical comparisons among the 4 groups were made using a 1-way ANOVA, followed by Student–Newman–Keuls analyses.

AmtB, or RhAG vs. day-matched H_2O oocytes. The right side of Fig. 5 shows that only for AQP1 oocytes was the mean P_f value significantly greater than that for H_2O oocytes; the P_f values for H_2O, AmtB, and RhAG oocytes were not significantly different from one another. Thus, despite the hypothesized presence of H_2O in the NH_3 pore of AmtB (20, 22), the 2 Rh proteins do not function as water channels.

Discussion

Channel-Dependent ΔpH_S and P_f Values. Given our experimental design, the magnitude of ΔpH_S is a semiquantitative index of both the flux of, and membrane permeability to, CO_2 or NH_3. For CO_2, the same is true of τ_{pHs}. Note that the quantitative relationship between ΔpH_S on the one hand and absolute flux or permeability on the other is likely to be different for CO_2 vs. NH_3. The portion of the CO_2-induced ΔpH_S signal that we can ascribe to a particular channel is the difference between the ΔpH_S of each channel-expressing oocyte (e.g., green record in Fig. 3*A*) and the ΔpH_S of its day-matched H_2O-injected control (e.g., orange record in Fig. 3*A*). Fig. 6*A* summarizes these differences, the channel-dependent signal $(\Delta pH_S^*)_{CO2}$, for the CO_2 data, computed oocyte by oocyte. Similarly, Fig. 6*B* summarizes the analogous differences, the channel-specific signal $(\Delta pH_S^*)_{NH3}$, for the NH_3 data. Note that the mean $(\Delta pH_S^*)_{NH3}$ values for AQP4 and AQP5 are not significantly different from zero.

Ratios of Indices of Permeability. Because we do not know the number of AQP molecules at the plasma membrane in each oocyte, it is impossible to normalize our $(\Delta pH_S^*)_{CO2}$ or $(\Delta pH_S^*)_{NH3}$ data to protein abundance. However, for each AQP oocyte, we also have a channel-dependent P_f (P_f^*), summarized in Fig. 6*C*. For each oocyte, we divided $(\Delta pH_S^*)_{CO2}$ or $(\Delta pH_S^*)_{NH3}$ by P_f^*. Fig. 6*D* summarizes these mean values, which represent semiquantitative indices of the CO_2/H_2O or NH_3/H_2O permeability ratios. By a factor of 2, AQP5 has the highest $(\Delta pH_S^*)_{CO2}/P_f^*$, and the values for AQP1 and AQP4 are indistinguishable.

Because we have both $(\Delta pH_S^*)_{CO2}$ and $(\Delta pH_S^*)_{NH3}$ for each of a large number of oocytes, it is also possible to compute the ratio $(\Delta pH_S^*)_{CO2}/(\Delta pH_S^*)_{NH3}$, a relative index of the CO_2/NH_3 permeability ratio, for AQP1, AmtB, and RhAG. Fig. 6*E* summarizes these values. Because $(\Delta pH_S^*)_{NH3}$ for AQP4 and AQP5 do not differ from zero, the ratios for these proteins are theoretically infinite. Thus, among the channels tested, AQP4 and AQP5 have the highest CO_2/NH_3 permeability ratios, followed by AQP1, AmtB, and RhAG. Conversely, RhAG has the highest NH_3/CO_2 permeability ratio (see Fig. S6).

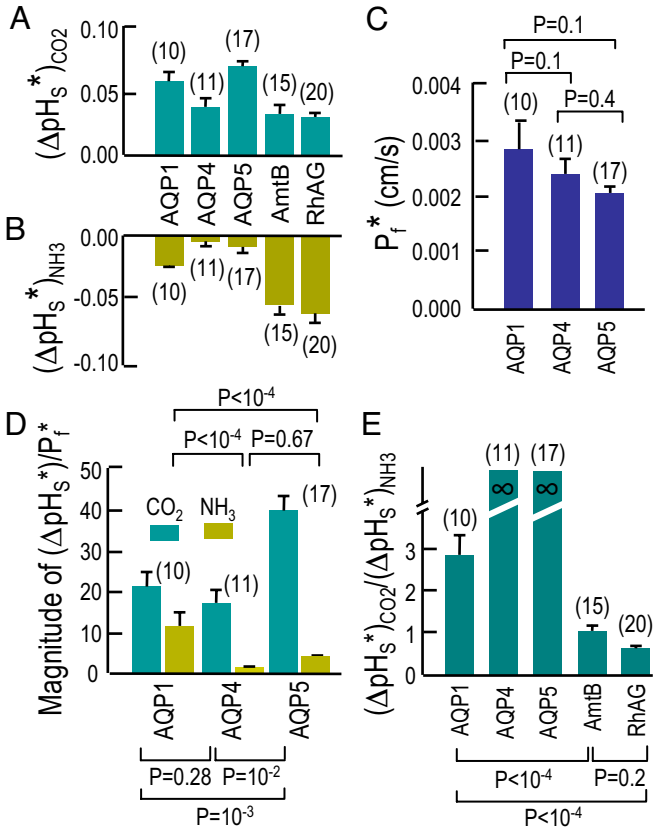

Fig. 6. Comparison of channel-dependent properties. (*A*) Indices of channel-dependent CO_2 permeability. For each ΔpH_S from a channel-expressing oocyte, we subtracted the mean, day-matched ΔpH_S for H_2O oocytes. Bars represent mean subtracted values, the channel-dependent ΔpH_S for CO_2, or $(\Delta pHS^*)_{CO2}$. Note: Oocytes in *A* are the same as those in *B* and *C*. (*B*) Indices of channel-dependent NH_3 permeability. We computed $(\Delta pH_S^*)_{NH3}$ using the same approach as in *A*. (*C*) Channel-dependent water permeabilities. For each P_f from a channel-expressing oocyte, we subtracted the mean, day-matched P_f for H_2O oocytes. Bars represent mean subtracted values, the channel-dependent P_f, or P_f^*. (*D*) Indices of channel-dependent CO_2 and NH_3 permeability, normalized to P_f^*. For each oocyte, we divided $(\Delta pH_S^*)_{CO2}$ and $(\Delta pH_S^*)_{NH3}$ by its P_f^*. (*E*) Indices of gas selectivity. For each oocyte expressing AQP1, AmtB, or RhAG, we divided $(\Delta pH_S^*)_{CO2}$ by $-(\Delta pH_S^*)_{NH3}$. Because $(\Delta pH_S^*)_{NH3}$ was not significantly different from zero for oocytes expressing AQP4 or AQP5, we represent these ratios as ''infinity.'' Statistical comparisons were made using 1-way ANOVAs for 3 groups, followed by Student–Newman–Keuls analyses.

Thus, compared with the AQPs tested, the Rh-like proteins tested are relatively more selective for NH_3, whereas the AQPs are relatively more selective for CO_2.

Significance. Our data demonstrate that channel proteins can exhibit gas selectivity by channel proteins. The basis of the selectivity is probably not the size of the transiting molecules—H_2O, CO_2, and NH_3 have similar minimum diameters—but rather their chemistries and the chemistries of the monomeric pores vs. the pore at the center of the multimers. The electronic configuration of NH_3 is identical to that of H_2O, which moves exclusively through the monomeric aquapores of AQP1. Thus, the hydrophilic NH_3 probably also moves exclusively through the monomeric aquapores of AQP1 and through the monomeric ammonia pores of AmtB and RhAG. The less hydrophilic CO_2, however, could move through the hydrophobic central pores of all 5 channels. NO is also known to move through AQP1 (8), and indirect evidence is consistent with the idea that O_2 moves

PHYSIOLOGY

through AQP1 (38). We suggest that the hydrophobic NO and O_2 move through the central pores. Crystallographic data show that xenon can enter the central pore of the bacterial Rh50 (21). Moreover, in the case of AQP1, molecular-dynamics simulations show that CO_2 could penetrate the 4 aquapores or, with greater ease, the central pore (7). We hypothesize that the CO_2/NH_3 selectivities that we observe reflect the relative permeabilities of the 2 gases through the monomeric vs. the central pores of the 5 channels we studied.

In a cell like the human RBC, whose plasma-membrane lipid has an intrinsically low gas permeability (6), the gas selectivity of AQP1 and the Rh complex would provide control over dissolved gases crossing the membrane. The NH_3 permeability of AQP1 and RhAG could enhance the ability of RBCs to pick up NH_3 in various tissues (where the NH_3 gradient would favor NH_3 uptake) and then to off-load it in the liver (where the gradient would favor NH_3 efflux from RBCs and uptake by hepatocytes) for NH_3 detoxification. In the hypertonic renal medulla, this NH_3 permeability could reduce the reflection coefficient for NH_3 and thereby reduce cell-volume changes. However, the low NH_3 permeability of AQP4 could protect the brain from rising blood levels of NH_3, while still allowing CO_2, and perhaps NO and O_2, to pass.

Materials and Methods

Molecular Biology. ***AQPs.*** Human AQP1 cDNA (GenBank accession no. NM_198098), cDNA encoding the rat AQP4/M23 splice variant (GenBank accession no. NM_012825), and human AQP5 cDNA (GenBank accession no. NM_012779) were gifts of Peter Agre (Johns Hopkins University, Baltimore).
AmtB. We cloned *E. coli* AmtB cDNA (GenBank accession no. ECU40429) by PCR from genomic DNA and subcloned the ≈1.3-kb PCR product into the *Xenopus* expression vector pGH19 (39). Using PCR, we created an additional construct in which we replaced the nucleotides encoding the signal sequence (i.e., first 22 residues) with ATG. At the 3′ end of some constructs, we added in-frame cDNA encoding either EGFP (Clontech, ref. 40) or a His tag.
RhAG. Human RhAG cDNA in pT7TS (GenBank accession no. NM_000324, a gift of Baya Chérif-Zahar, Université René Descartes, INSERM, Paris) (41) was subcloned into pGH19. We tagged RhAG at its 3′ end with EGFP.
Other cDNAs. Rabbit NKCC2 (42) was a gift of Biff Forbush (Yale University, New Haven, CT). SGLT1 (43) and PepT1 (44) were gifts of Matthias Hediger (Brigham and Women's Hospital and Harvard Medical School, Boston).

Site-Directed Mutagenesis. We used the QuikChange Site-Directed Mutagenesis Kit (Stratagene), following the manufacturer's instructions.

cRNA Preparation. We generated cRNA using the Message Machine kit (Ambion) and, unless otherwise stated, injected oocytes with 50 nL of 0.5 ng/nL of cRNA or 25 nL of 1 ng/nL of cRNA.

Western Blot Analysis. Plasma-membrane proteins were prepared from oocytes (45), separated on a 13% SDS polyacrylamide gel, blotted on a PVDF membrane, probed with a monoclonal anti-His antibody (Catalog no. 70796–3, Novagen), and detected using ECL plus Western Blotting Detection Reagents (Amersham Biosciences).

Solutions for Physiological Assays. The ND96 solution contained: 96 mM NaCl, 2 mM KCl, 1 mM $MgCl_2$, 1.8 mM $CaCl_2$, and 5 mM Hepes, pH 7.50, osmolality 195 mOsm. For P_f assays, we used a hypotonic ND96 variant (100 mOsm) that contained only 43 mM NaCl. The CO_2/HCO_3^- solution was identical to ND96 except that 33 mM $NaHCO_3$ replaced 33 mM NaCl, and the solution was bubbled with 5% CO_2/balance O_2. The NH_3/NH_4^+ solution was a variant of ND96 in which we replaced 0.5 mM NaCl with 0.5 mM NH_4Cl. The butyrate solution was a variant of ND96 in which we replace 30 mM Na-butyrate with 30 mM NaCl.

Carbonic-Anhydrase Assay. Carbonic-anhydrase activity was assessed in 20 μg of membrane preparation of CA-IV or AQP1 oocytes using a colorimetric technique (46). The assay measures the rate at which the pH of a weakly buffered alkaline solution (imidazole-Tris, 50% CO_2, with p-nitrophenol as indicator at 0 °C), falls in the presence or absence of CA, noted by a color change from yellow to clear, due to the reaction $CO_2 + H_2O \rightarrow HCO_3^- + H^+$.

Measurement of Oocyte Water Permeability. We used a volumetric assay (47, 48) to measure osmotic water permeability (P_f). Briefly, after dropping oocytes into a Petri dish containing the hypotonic solution, we acquired video images every 1–2 s, obtaining the time course of the projection area of the oocyte. Assuming the oocyte to be a sphere, and the true surface area (S) to be 8-fold greater than the idealized area (49), we computed P_f as:

$$P_f = \frac{V_o \cdot \frac{d(V/V_o)}{dt}}{S \cdot \Delta Osm \cdot V_w}$$

where V_o is initial oocyte volume, $d(V/V_o)/dt$ is the maximal fractional rate of volume increase, ΔOsm is the osmotic gradient across the membrane, and V_w is the molar volume of water.

Measurement of Surface pH. We used microelectrodes to measure pH_S (6, 50). Briefly, the pH electrode had a tip diameter of 15 μm, was filled at its tip with H^+ ionophore mixture B (Catalog no. 95293, Fluka), and was connected to a FD223 electrometer (World Precision Instruments). The extracellular reference electrode was a glass micropipette filled with 3 M KCl and connected via a calomel half cell to a 750 electrometer (World Precision Instruments). The extracellular solution flowed at 3 mL/min, and the sampling rate was 1 per 500 ms. Using an MPC-200 system micromanipulator (Sutter Instrument), we positioned the pH_S electrode tip either in the bulk extracellular fluid or dimpling ≈40 μm onto the oocyte surface, in the ''shadow'' of the oocyte. Although not displayed in the figures, membrane potential (V_m) and intracellular pH were also monitored (see *SI Text*). All oocytes had initial V_m values at least as negative as −40 mV.

We verified delivery of EGFP-tagged proteins to a region near the plasma membrane by using a 96-well plate reader (BMG Labtechnologies) to assess fluorescence (40).

Data Analysis. Before applying CO_2/HCO_3^- or NH_3/NH_4^+, we computed pH_S from the preceding calibration, with the electrode tip in the bulk phase of the ND96 solution (pH 7.50). After applying CO_2/HCO_3^- or NH_3/NH_4^+, we computed pH_S from a second calibration in the bulk phase of the new solution (also pH 7.50). The maximum pH_S excursion (ΔpH_S) was taken as the maximum pH_S after the application of CO_2/HCO_3^- (or the minimum pH_S after application of NH_3/NH_4^+) minus the pH_S prevailing just before the solution change from ND96.

Statistics. Data are presented as mean ± SEM. To compare the difference between 2 means, we performed Student's *t* tests (two tails). To compare more than 2 means, we performed a 1-way ANOVA followed by a Dunnett's or a Student–Newman–Keuls posthoc analysis, using KaleidaGraph (Version 4, Synergy Software). $P < 0.05$ was considered significant.

ACKNOWLEDGMENTS. We thank Drs. Baya Chérif-Zahar, Peter Agre, Matthias Hediger, and Biff Forbush for providing cDNA or cRNA. Duncan Wong provided computer support. Mark Parker and Lara Skelton provided helpful discussions. This work was supported by Grant 1N00014-05-0345 (Office of Naval Research, to W.F.B.). For part of the period (from 07/2006 to 10/2007), R.M.A. was supported by a fellowship from the American Heart Association (0625891T).

1. Waisbren SJ, *et al.* (1994) Unusual permeability properties of gastric gland cells. *Nature* 368:332–335.
2. Nakhoul NL, *et al.* (1998) Effect of expressing the water channel aquaporin-1 on the CO_2 permeability of *Xenopus* oocytes. *Am J Physiol* 274:C543–C548.
3. Cooper GJ, Boron WF (1998) Effect of pCMBS on CO_2 permeability of *Xenopus* oocytes expressing aquaporin 1 or its C189S mutant. *Am J Physiol* 275:C1481–C1486.
4. Prasad GV, *et al.* (1998) Reconstituted aquaporin 1 water channels transport CO_2 across membranes. *J Biol Chem* 273:33123–33126.
5. Uehlein N, *et al.* (2003) The tobacco aquaporin NtAQP1 is a membrane CO_2 pore with physiological functions. *Nature* 425:734–737.
6. Endeward V, *et al.* (2006) Evidence that Aquaporin 1 is a major pathway for CO_2 transport across the human erythrocyte membrane. *FASEB J* 20:1974–1981.
7. Wang Y, *et al.* (2007) Exploring gas permeability of cellular membranes and membrane channels with molecular dynamics. *J Struct Biol* 157:534–544.
8. Herrera M, Hong NJ, Garvin JL (2006) Aquaporin-1 transports NO across cell membranes. *Hypertension* 48:157–164.
9. Nakhoul NL, *et al.* (2001) Transport of NH_3/NH_4^+ in oocytes expressing aquaporin-1. *Am J Physiol* 281:F255–F263.
10. Holm LM, *et al.* (2005) NH_3 and NH_4^+ permeability in aquaporin-expressing *Xenopus* oocytes. *Pflügers Arch* 450:415–428.

11. Saparov SM, *et al.* (2007) Fast and selective ammonia transport by aquaporin-8. *J Biol Chem* 282:5296–5301.
12. Peng J, Huang CH (2006) Rh proteins vs Amt proteins: An organismal and phylogenetic perspective on CO_2 and NH_3 gas channels. *Transfusion Clin Biol* 13:85–94.
13. Winkler FK (2006) Amt/MEP/Rh proteins conduct ammonia. *Pflügers Arch* 451:701–707.
14. Khademi S, Stroud RM (2006) The Amt/MEP/Rh family: Structure of AmtB and the mechanism of ammonia gas conduction. *Physiology (Bethesda)* 21:419–429.
15. Soupene E, Lee H, Kustu S (2002) Ammonium/methylammonium transport (Amt) proteins facilitate diffusion of NH_3 bidirectionally. *Proc Natl Acad Sci USA* 99:3926–3931.
16. Marini AM, *et al.* (1994) Cloning and expression of the MEP1 gene encoding an ammonium transporter in *Saccharomyces cerevisiae. EMBO J* 13:3456–3463.
17. Fabiny JM, *et al.* (1991) Ammonium transport in *Escherichia coli*: Localization and nucleotide sequence of the amtA gene. *J Gen Microbiol* 137:983–989.
18. Zheng L, *et al.* (2004) The mechanism of ammonia transport based on the crystal structure of AmtB of *Escherichia coli. Proc Natl Acad Sci USA* 101:17090–17095.
19. Khademi S, *et al.* (2004) Mechanism of ammonia transport by Amt/MEP/Rh: Structure of AmtB at 1.35 angstrom. *Science* 305:1587–1594.
20. Conroy MJ, *et al.* (2007) The crystal structure of the Escherichia coli AmtB-GlnK complex reveals how GlnK regulates the ammonia channel. *Proc Natl Acad Sci USA* 104:1213–1218.
21. Lupo D, *et al.* (2007) The 1.3-A resolution structure of Nitrosomonas europaea Rh50 and mechanistic implications for NH_3 transport by Rhesus family proteins. *Proc Natl Acad Sci USA* 104:19303–19308.
22. Andrade SL, *et al.* (2005) Crystal structure of the archaeal ammonium transporter Amt-1 from Archaeoglobus fulgidus. *Proc Natl Acad Sci USA* 102:14994–14999.
23. Ripoche P, *et al.* (2004) Human Rhesus-associated glycoprotein mediates facilitated transport of NH_3 into red blood cells. *Proc Natl Acad Sci USA* 101:17222–17227.
24. Soupene E, Inwood W, Kustu S (2004) Lack of the Rhesus protein Rh1 impairs growth of the green alga *Chlamydomonas reinhardtii* at high CO_2. *Proc Natl Acad Sci USA* 101:7787–7792.
25. Endeward V, *et al.* (2008) RhAG protein of the Rhesus complex is a CO_2 channel in the human red cell membrane. *FASEB J* 22:64–73.
26. De Hemptinne A, Huguenin F (1984) The influence of muscle respiration and glycolysis on surface and intracellular pH in fibres of the rat soleus. *J Physiol* 347:581–592.
27. Chesler M (1986) Regulation of intracellular pH in reticulospinal neurones of the lamprey, Petromyzon Marinus. *J Physiol* 381:241–261.
28. Blank ME, Ehmke H (2003) Aquaporin-1 and HCO_3^--Cl^- transporter-mediated transport of CO_2 across the human erythrocyte membrane. *J Physiol* 550:419–429.
29. Nagelhus EA, Mathiisen TM, Ottersen OP (2004) Aquaporin-4 in the central nervous system: Cellular and subcellular distribution and coexpression with KIR4.1. *Neuroscience* 129:905–913.
30. Verkman AS, Matthay MA, Song Y (2000) Aquaporin water channels and lung physiology. *Am J Physiol* 278:L867–L879.
31. Ridgwell K, *et al.* (1992) Isolation of cDNA clones for a 50 kDa glycoprotein of the human erythrocyte membrane associated with Rh (rhesus) blood-group antigen expression. *Biochem J* 287:223–228.
32. Musa-Aziz R, *et al.* (2009) Concentration-dependent effects on intracellular and surface pH of exposing *Xenopus* oocytes to solutions containing NH_3/NH_4^+. *J Membr Biol*, in press.
33. Parker MD, *et al.* (2008) Characterization of human SLC4A10 as an electroneutral Na/HCO3 cotransporter (NBCn2) with Cl- self-exchange activity. *J Biol Chem* 283:12777–12788.
34. Javelle A, *et al.* (2004) Ammonium sensing in *Escherichia coli.* Role of the ammonium transporter AmtB and AmtB-GlnK complex formation. *J Biol Chem* 279:8530–8538.
35. Marini AM, *et al.* (2006) Structural involvement in substrate recognition of an essential aspartate residue conserved in Mep/Amt and Rh-type ammonium transporters. *Curr Genet* 49:364–374.
36. Thomas GH, Mullins JGL, Merrick M (2000) Membrane topology of the Mep/Amt family of ammonium transporters. *Mol Microbiol* 37:331–344.
37. Thornton J, *et al.* (2006) The ammonia channel protein AmtB from *Escherichia coli* is a polytopic membrane protein with a cleavable signal peptide. *FEMS Microbiol Lett* 258:114–120.
38. Echevarria M, *et al.* (2007) Development of cytosolic hypoxia and hypoxia-inducible factor stabilization are facilitated by aquaporin-1 expression. *J Biol Chem* 282:30207–30215.
39. Trudeau MC, *et al.* (1995) HERG, a human inward rectifier on the voltage-gated potassium channel family. *Science* 269:92–95.
40. Toye AM, *et al.* (2006) The human NBCe1-A mutant R881C, associated with proximal renal tubular acidosis, retains function but is mistargeted in polarized renal epithelia. *Am J Physiol* 291:C788–C801.
41. Marini AM, *et al.* (2000) The human Rhesus-associated RhAG protein and a kidney homologue promote ammonium transport in yeast. *Nat Genet* 26:341–344.
42. Payne JA, Forbush B (1994) Alternatively Spliced Isoforms of the Putative Renal Na-K-Cl Cotransporter Are Differentially Distributed Within the Rabbit Kidney. *Proc Natl Acad Sci USA* 91:4544–4548.
43. Hediger MA, *et al.* (1987) Expression cloning and cDNA sequencing of the Na^+/glucose co-transporter. *Nature* 330:379–381.
44. Fei YJ, *et al.* (1994) Expression cloning of a mammalian proton-coupled oligopeptide transporter. *Nature* 368:563–566.
45. Leduc-Nadeau A, *et al.* (2007) Elaboration of a novel technique for purification of plasma membranes from *Xenopus laevis* oocytes. *Am J Physiol* 292:C1132–C1136.
46. Brion LP, *et al.* (1988) Micro-Method for the measurement of carbonic anhydrase activity in cellular homogenates. *Anal Biochem* 175:289–297.
47. Virkki LV, *et al.* (2002) Cloning and functional characterization of a novel aquaporin from *Xenopus laevis* oocytes. *J Biol Chem* 277:40610–40616.
48. Preston GM, *et al.* (1993) The mercury-sensitive residue at cysteine 189 in the CHIP28 water channel. *J Biol Chem* 268:17–20.
49. Chandy G, *et al.* (1997) Comparison of the water transporting properties of MIP and AQP1. *J Membr Biol* 159:29–39.
50. Musa-Aziz R, Grichtchenko II, Boron WF (2005) (2005) Evidence from surface-pH transients that CA IV and CAII enhances CO_2 influx into X*enopus* oocytes. *J Am Soc Nephrol* 16:P0015.